Photosensitization of TiO_2 and SnO_2 by Artificial Self-Assembling Mimics of the Natural Chlorosomal Bacteriochlorophylls

Annemarie Huijser,[†] Peter L. Marek,[‡,||] Tom J. Savenije,[†] Laurens D.A. Siebbeles,[†] Torsten Scherer,[‡] Robert Hauschild,[§] Jędrzej Szmytkowski,[§] Heinz Kalt,[§] Horst Hahn,[‡,||] and Teodor Silviu Balaban*[,‡]

Opto-Electronic Materials Section, DelftChemTech, Delft University of Technology, Julianalaan 136, 2628 BL, Delft, The Netherlands, Karlsruhe Institute of Technology (KIT), Forschungszentrum Karlsruhe (FZK), Institute for Nanotechnology (INT), Postfach 3640, D-76021 Karlsruhe, Germany, Center for Functional Nanostructures (CFN), University of Karlsruhe (TH), D-76021 Karlsruhe, Germany, Karlsruhe Institute of Technology, Universität Karlsruhe (TH), D-76021 Karlsruhe, Germany, and Fakultät für Angewandte Physik and Joint Research Laboratory Nanomaterials, TU-Darmstadt and Forschungszentrum Karlsruhe, Petersenstrasse 23, 64287 Darmstadt, Germany

Received: April 15, 2007; In Final Form: May 17, 2007

Of all known photosynthetic organisms, the green sulfur bacteria are able to survive under the lowest illumination conditions due to highly efficient photon management and exciton transport enabled by their special organelles, the chlorosomes, which consist mainly of self-assembled bacteriochlorophyll *c*, *d*, or *e* molecules. A challenging task is to mimic the principle of self-assembling chromophores in artificial light-harvesting devices. In the present work we have studied exciton transport and dissociation in a bilayer of an electron-accepting semiconductor and an artificial self-assembling zinc porphyrin that mimics natural chlorosomal bacteriochlorophylls using time-resolved microwave conductivity (TRMC). Scanning electron microscopy (SEM) reveals the presence of large domains with dimensions up to several micrometers that consist of self-assembled stacks. In addition to these large self-assembled stacks, absorption and fluorescence spectra reveal the presence of monomers. The fluorescence in the solid state, just as in the chlorosomes, is only partially quenched and its decay shows two components, one with lifetimes of 40 ps stemming from the aggregates and a longer one with 2.5 ns lifetime ascribed to monomeric zinc porphyrins. Predominantly those photons that are absorbed by the monomers lead to the formation of charge-separated states. The rather low contribution of self-assembled stacks to the formation of charge-separated states, most likely, results from their interaction with the semiconductor, combined with the presence of monomers at the semiconductor surface and the energetically unfavorable exciton transfer from a stack to a monomer. However, we prove herein that biomimetic self-assembling porphyrins can be used to photosenzitize wide band gap semiconductors as a 2.2% incident photon to charge separation efficiency could be measured. Realizing an ordered structure of stacks in proper contact with the electron-accepting semiconductor will probably improve their contribution to the formation of charge-separated states. This might pave the way to cost-efficient hybrid solar cells using artificial chlorosome-like antenna architectures, allowing them to work also under dim or diffuse light.

Introduction

The high efficiency of photosynthetic processes is due to an optimized photon capture mechanism coupled to a vectorial energy transfer which is determined by the specific orientation of the chromophore molecules that are present in light-harvesting systems. After trapping the light energy, charge separation occurs within reaction centers, and by successive electron transfer steps, the hole and electron eventually become separated on opposite sides of the photosynthetic membrane. In general, light-harvesting (or antenna) systems are based on chromophore−protein complexes, in which the proteinaceous scaffold determines the orientation of the chromophore molecules.[1] This specific orientation ensures an efficient transport of the excitation energy toward the reaction center so that almost every photon captured by the antenna eventually can have its energy trapped.[2] An exception to chromophore−protein based light-harvesting systems is the chlorosome: an extramembraneous, cigar-shaped, and roughly 15 × 30 × 100 nm sized organelle, which is present in green sulfur bacteria as well as in filamentous bacteria.[3] In chlorosomes bacteriochlorophyll (BChl) *c*, *d*, or *e* molecules (Chart 1) self-assemble without the aid of proteins.[4−6] Essential for self-assembly are (i) the ligation of the central magnesium atom by the 3^1-hydroxy group of an adjacent molecule, (ii) the $\pi-\pi$ interactions between the macrocycles, and (iii) a weak interaction of the 13^1-carbonyl group with the central Mg atom of a third BChl. It was previously thought that a hydrogen bonding interaction is operating,[4−6] but recently, using single-crystal diffraction, we have discovered that a similar carbonyl group weakly ligates a porphyrinic central metal atom and is thus unavailable for further H-bonding.[7] Based upon such self-assembling porphyrins which are BChl mimics (Chart 1), a new model for the chlorosomal self-assemblies was proposed.[7e]

* Corresponding author. Fax: +49 724 782 8298. E-mail: silviu.balaban@int.fzk.de.
[†] DelftChemTech.
[‡] KIT, FZK-INT, and CFN.
[§] KIT, Angewandte Physik, and CFN.
[||] Joint Research Laboratory Nanomaterials, TU-Darmstadt and FZK.

10.1021/jp072927s CCC: $37.00 © 2007 American Chemical Society
Published on Web 07/17/2007

CHART 1: Naturally Occurring Chlorosomal Bacteriochlorophylls (Left) and Our Self-Assembling Mimic 1 (Right)[a]

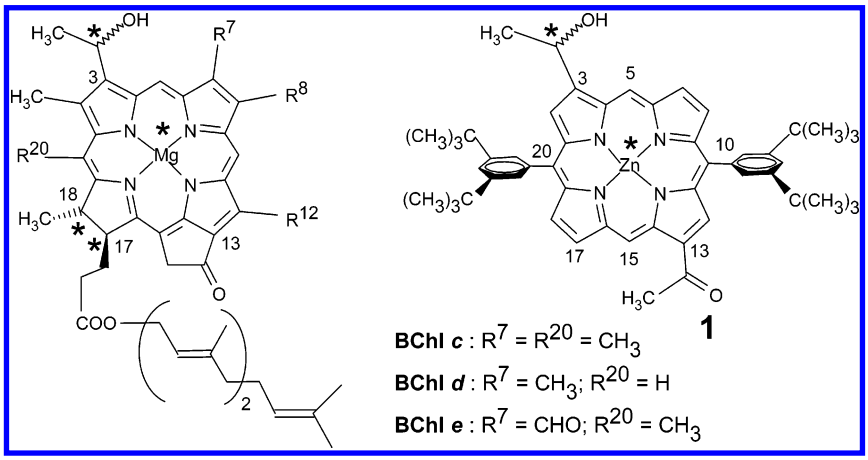

[a] The isomeric mimic **2** has the 1-hydroxyethyl and acetyl groups in the meso positions (5 and 15, respectively). The residues R^8 can be methyl, ethyl, propyl, or isobutyl, while the residues R^{12} can be methyl or ethyl. Farnesol is here depicted as the long-chain fatty alcohol esterifying the 17-propionic acid residue. However, cetol, stearol, geranyl-geraniol, phytol, or oleanol may be also encountered in various photosynthetic bacteria within chlorosomes. Asterisks denote stereogenic centers which include the metal atoms within self-assemblies where the 3^1-hydroxy group coordinates the magnesium or zinc atoms. Both 3^1-(*R*) and -(*S*) epimers are naturally occurring although in different amounts which depend upon the illumination conditions. Racemic **1** was employed in the present study.

Porphyrins are synthetic chromophores related to BChls having a fully conjugated π-periphery of the tetrapyrrolic macrocycle and are available in large quantities by various methods.[8] BChl's have a 17, 18 single bond, and most importantly, the annulated five-membered ring ensures that the 13^1-carbonyl group cannot deviate very much from the tetrapyrrolic plane.

Self-assembly affects the optical properties of the bacteriochlorophyll *c* molecules and results in an efficient energy transfer pathway through the chlorosome to the energetic trap, consisting of a trimeric BChl *a* containing protein, the so-called Fenna−Matthew−Olson complex, which is closely coupled to the reaction center.[1i−k] Of all known photosynthetic organisms the green sulfur bacteria are able to survive under the lowest illumination conditions, such as 80 m under the water surface in the Black Sea,[9a] or even at an 2380 m oceanic depth near a "Black Smoker" volcanic vent.[9b] These latter BChl *c* containing phototrophs are thus unique in being able to harvest near-infrared radiation which does not originate from the sun, and this illustrates the tremendous light-harvesting efficiency of their chlorosomes.

A challenging task is to mimic the principle of self-assembling chromophores in an artificial light-harvesting device as the presently available silicon-based photovoltaic devices fail to function under low or diffuse light illumination conditions. Coupling a self-assembling antenna, which increases both the photon capture cross section and the wavelength range, to a photovoltaic device might improve the overall efficiency while ensuring cheap manufacturing costs. The concept of exciton dissociation into charge-separated states within the reaction center shows considerable similarities with dye-sensitized solar cells.[10] The key feature of these injection, or "Grätzel" solar cells is the efficient exciton dissociation at the interface of the dye and the electron-accepting semiconductor, leading to very fast injection of an electron into the conduction band of the semiconductor.[11] Since O'Regan and Grätzel reported an efficiency higher than 7% for a cell based on an interpenetrating network of dye-coated nanocrystalline TiO_2 particles and a liquid electrolyte, such nanostructured systems have been studied extensively, and their efficiencies have been constantly improved.[12] Because of complications involved in the use, sealing, and servicing of a liquid electrolyte, current research is focused on the development of all solid-state, flexible solar cells, for which a maximum performance of 4% has been realized so far.[13] These cells can now be manufactured with cheap roll-to-roll processes known from the polymer, packaging, and printing industries. Very recently, Grätzel and collaborators have reported a 7.2% efficiency of a flexible dye-sensitized solar cell using a Ti metal foil substrate for a nanocrystalline TiO_2 photoanode.[14] Application of nanostructured systems avoids the necessity of efficient long-range exciton transport through the dye layer. However, in such systems electron transport is hindered due to trapping at surface defect states.[15] The difficulties involved in electron transport can be avoided by application of dye and electron-accepting semiconductor in a bilayer configuration. A prerequisite for an efficient bilayer-based solar cell is the presence of an exciton transport pathway across the dye layer and the interface with the electron-accepting semiconductor. This may be realized with self-assembling chromophores in artificial chlorosomal architectures.

Experimental Section

Sample Preparation. Thin smooth TiO_2 films with a thickness of ca. 100 nm, prepared by chemical vapor deposition onto $1 \times 12 \times 25$ mm^3 quartz substrates, were purchased from Everest Coatings, Delft, The Netherlands. Thin smooth SnO_2 films with a thickness of ca. 200 nm, prepared by reactive magnetron sputtering, are a generous gift of the Fraunhofer Institut für Elektronenstrahl- und Plasmatechnik, Dresden, Germany. Racemic 3-(1-hydroxyethyl)-13-acetyl-10,20-bis(3,5-di-*tert*-butylphenyl)porphinato zinc (**1**) was synthesized as previously described.[7] The chemical structure of **1** is shown in Chart 1. Since anhydrous conditions are essential for self-assembly, solvents were thoroughly dried in advance. Dichloromethane was distilled from calcium hydride and *n*-heptane was distilled from sodium metal, both under nitrogen atmosphere. The heterochiral self-assembly is favored over a homochiral one as the separated enantiomers of **1** showed a drastically decreased formation of aggregates.[7d] Porphyrin film deposition was performed by spin-coating from a solution in dry dichloromethane at 2500 rpm. Annealing treatments were performed at a temperature of 200 °C for a period of 15 min in an oven. Both film deposition and annealing treatments were performed under nitrogen atmosphere, with H_2O and O_2

concentrations below 10 ppm using a glovebox. Porphyrin film thicknesses were determined using a Veeco Dektak 8 Stylus Profiler and found to be 150 ± 5 nm, 90 ± 5 nm, and 140 ± 5 nm for **1** spin-coated on TiO_2, SnO_2, and quartz substrates, respectively.

Scanning Electron Microscopy. Scanning electron micrographs were recorded using a Leo 1530 Gemini scanning electron microscope (SEM), operated at an accelerating voltage of 20 kV. Samples were sputtered with a 6 nm Pt film prior to SEM investigation; however, for higher acceleration voltages sputtering was not required on conductive substrates as the aggregates in themselves are conductive.

Optical Characterization. Optical transmission spectra of **1** as solutions were recorded in Delft using a Perkin-Elmer Lambda 40 UV−vis spectrophotometer. Optical transmission and reflection spectra of thin films were recorded with a Perkin-Elmer Lambda 900 UV/vis/NIR spectrophotometer, using an integrating sphere. From the transmission and reflection spectra, the optical density (OD) and the fraction of absorbed light (F_A) were determined using eqs 1 and 2, with I_T the intensity of the transmitted light, I_0 the incident light intensity, and I_R the intensity of the reflected light:

$$\mathrm{OD} = -\log\left(\frac{I_T}{I_0 - I_R}\right) \quad (1)$$

$$F_A = 1 - \left(\frac{I_T + I_R}{I_0}\right) \quad (2)$$

The wavelength dependences of OD and F_A are referred to as the OD spectrum and the attenuation spectrum, respectively. Alternatively, absorption spectra in solution were measured in Karlsruhe on a Varian-Cary 500 UV−vis−NIR spectrometer using quartz cuvettes having path lengths of 0.01−1.0 cm and alternatively using an integrating sphere.

Photoconductivity Measurements. The TRMC technique and experimental setup have been described previously.[16,23] Samples were mounted in an X-band microwave cavity at a position of maximum electric field. Experiments were performed under N_2 atmosphere. Samples were illuminated through the quartz substrate, resulting in a high initial exciton concentration near the exciton-dissociating interface between the **1** layer and TiO_2 or SnO_2. The incident intensity was varied between 1×10^{10} and 1×10^{14} photons/cm^2 per pulse. The laser pulse has a full width at half-maximum equal to 3 ns.

The data analysis has been described earlier.[16] Briefly, the formation of mobile charge carriers due to pulsed illumination leads to an increase of the photoconductance (ΔG), followed by an eventual decrease caused by the decay of charge carriers. Note that the current experiments were carried out in the absence of charge-collecting electrodes. This implies that decay of the photoconductance is not due to the extraction of charge carriers. From the maximum of the photoconductance (ΔG_{max}), the incident photon to charge separation efficiency (IPCSE) was calculated as described in the literature.[16] The IPCSE represents the ratio of the number of electrons injected into the electron-accepting semiconductor to the number of incident photons.

Time-Resolved Fluorescence. For the time-resolved-fluorescence measurements a Ti:sapphire laser delivering sub-150 fs pulses at a repetition rate of 76 MHz was used. The compound second harmonic generation was excited by using a BBO. Selective excitation of either the monomers or the aggregates could be performed by tuning the wavelength at 419 or 447 nm, respectively. The spectral width of the pulses was about 5 nm so that excitation conditions are comparable to that of Figure 2A. A closed loop circulation system consisting of an optics cuvette and a peristaltic pump was used to minimize photodegradation by assuring a continuous flow. The fluorescence signal was detected by a streak camera (Hamamatsu C5680) coupled to a spectrometer (Jobin-Yvon HR460, 100 lines/mm grating). Fluorescence spectra were measured in the wavelength range between 580 and 755 nm, with a spectral resolution of 2 nm and a temporal resolution of 8 ps. A polarizer was used to compensate the effect of molecular rotation on the fluorescence decay.

Results and Discussion

In the present article we report on the exciton transport and dissociation in a bilayer of an electron-accepting semiconductor and an artificial self-assembling zinc porphyrin (see Chart 1) that mimics natural chlorosomal bacteriochlorophylls.[7] The presence of self-assembled porphyrin stacks has been verified using scanning electron microscopy (SEM), fluorescence, and optical absorption. Exciton transport and dissociation, resulting in the formation of charge-separated states, has been studied using time-resolved microwave conductivity (TRMC) measurements.[16] In previous studies we performed confocal fluorescence microscopy of **1** self-assembled on nanocrystalline titania (anatase)[7c] and recorded small-angle X-ray scattering (SAXS) spectra of films of **1** (vide infra).[7d]

Figure 1 shows the absorption spectrum of 13-acetyl-3-(1-hydroxyethyl)-10,20-bis(3,5-di-*tert*-butylphenyl)porphinato zinc (**1**) in various solvents as well as in the solid aggregated state. The strong Soret band around 430 nm and the less intense Q-bands at 565 and 610 nm are characteristic absorption bands for zinc porphyrin monomers.[17] Note that in commercial dichloromethane, which contains 0.2% ethanol as stabilizer, no self-assembly occurs. In nonpolar solvents such as *n*-heptane, cyclohexane, or *n*-hexane, self-assembly is induced as put into evidence by major changes in the absorption and fluorescence spectra.[7a] Broad and red-shifted absorption maxima in comparison to the monomers indicate self-assembly as in J-aggregates,[18] with a considerable size distribution responsible for the observed inhomogeneous broadening. The Soret bands of the aggregates peak at 480 nm while one of the Q bands, characteristic for self-assembled **1**, is at 637 nm and originates from self-assembling stacks.[7b−e] For light harvesting, the broad absorption features are beneficial as they allow photon capture from 300 nm to almost 700 nm. Self-assembly of **1** has been realized by the rapid injection of its concentrated solution in dry CH_2Cl_2 into a large excess of dry *n*-heptane at room temperature. The ratio of CH_2Cl_2 to *n*-heptane corresponded to 1:20 (for materials and methods, see also the Supporting Information). The absorption band at 422 nm results from a residual amount of monomeric **1**. Addition of a minute, but suprastoichiometric amount of a solvent that competes for the metal ligation, such as pyridine or (m)ethanol, to this solution disrupts the self-assemblies and results in the presence of predominantly monomeric **1** ligated by pyridine or (m)ethanol, respectively.

Figure 1B shows the optical density (OD) spectrum of **1** spin-coated from a solution in CH_2Cl_2 on a flat TiO_2 substrate. The film thickness, as determined by profilometry, had an average value of about 150 nm. The absorption band below 350 nm originates from TiO_2. In analogy with the absorption spectra discussed above, the broad absorption bands at 495, 575, and 628 nm originate from self-assembled stacks of **1**. Annealing at 200 °C for 15 min only slightly lowers the monomer

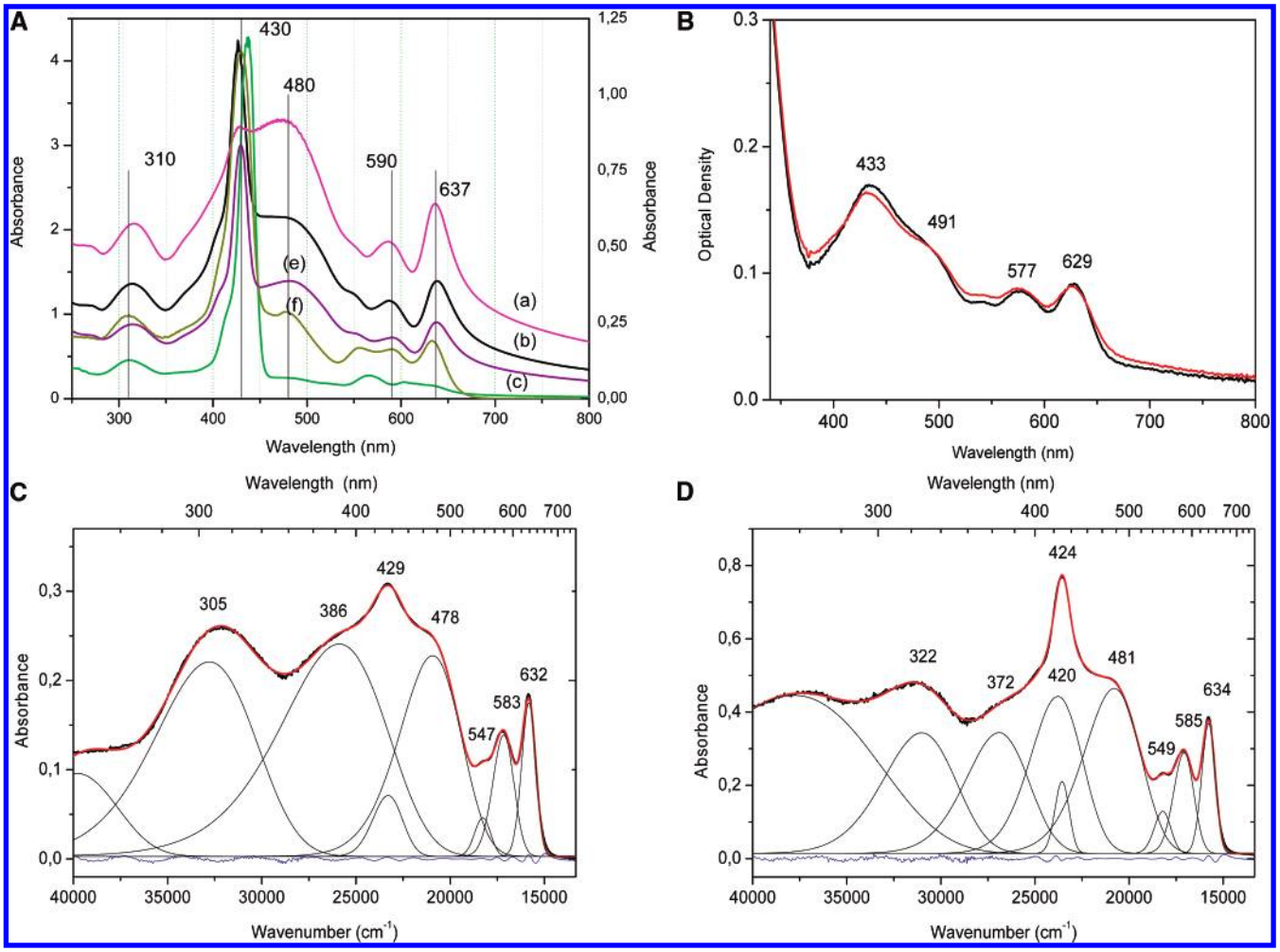

Figure 1. (A) Absorption spectra of **1** in different solvents. The right ordinate axis refers to traces a−c, while the left ordinate axis refers to traces e and f. (a) **1** (∼0.2 mg) dissolved in a minimum amount of dry dichloromethane (100 μL) which was then diluted in 2 mL of dry *n*-heptane, path length 1 cm. (b) and (c) Solutions in dry dichloromethane and commercial dichloromethane, respectively. Note that in commercial dichloromethane only monomers are present, whereas in dry dichloromethane, or especially after dilution in a large excess of dry *n*-heptane, aggregate maxima at 480 and 637 nm are prominent. Due to light scattering caused by aggregates larger than 100 nm, the baseline is shifted in the corresponding spectra. This shift is absent in trace f, which was a dry dichloromethane solution measured in an integrating sphere. Trace e represents a solution in commercial dry diethyl ether. (B) Optical density spectra of **1** self-assembled on a flat TiO_2 electrode, before (black trace) and after annealing (red trace) at 200 °C for 15 min (see also the Supporting Information, Figure S1). (C) Absorption spectrum measured in an integrating sphere from a film of **1** deposited on the walls of a quartz cuvette from *n*-heptane. Thick black trace, experimental spectrum; red trace, fit with eight Gaussian components; blue trace, residuals. (D) Absorption spectrum measured in an integrating sphere of **1** (∼0.1 mg) dissolved in 200 μL of dry dichloromethane which was then diluted in 1.8 mL of dry *n*-heptane. Noisy black trace, experimental spectrum; red trace, fit with nine Gaussian components; blue trace, residuals. All peak parameters (width and wavelength) were allowed to vary freely. Note that more monomers are present than in (C). Characteristic aggregate peaks are at 634 and 481 nm.

absorption band. Since untreated and annealed **1** dissolved in CH_2Cl_2 exhibit identical OD spectra, the occurrence of chemical degradation upon annealing is ruled out (see also Supporting Information Figure S1). The surprisingly high thermal and temporal stability of the self-assemblies allows prolonged heating at 220 °C in an inert atmosphere, or even irradiation with an electron beam at high accelerating voltages (20 kV) in a vacuum. Hardly any changes in the absorption spectra or images are encountered (see Supporting Information Figures S1 and S2). Potential thermal dehydration of the 3-hydroxyethyl group, even at 235 °C, apparently is inhibited by aggregation and lack of an acidic catalyst. Figure 1C shows the absorption spectrum of a thin film of **1** deposited on the walls of a 1 cm quartz cuvette from *n*-heptane together with a deconvolution which gave an acceptable fit. Fewer components lead to a significantly poorer agreement. Noteworthy are the broad components typical for the aggregate bands at 480 and 631 nm and the monomer Soret band at 429 nm. A broad component blue-shifted from the monomers is also found by the fitting procedure at ∼385 nm, and this could be the high-energy band of a Davidov split aggregate transition. This peak is considerably smaller in the absorption spectra of aggregate samples suspended in *n*-heptane and is thus ascribable to the film formation. Figure 1D presents the experimental spectrum of such an *n*-heptane suspension and similar Gaussian band decomposition as in Figure 1C. Note the more prominent monomer maximum, and a smaller high energy aggregate band. A slight red shift of the aggregate bands occurs in the suspension in comparison to the film, while the monomer Soret band is blue-shifted by 5 nm. A strong baseline drift is due to the scattering contribution of the large aggregate particles, and this can be eliminated by measuring the suspension in an integrating sphere.

Fluorescence spectra recorded in the solid state show a broad maximum at 655 nm having a large Stokes shift (∼25 nm, compared to the 637 nm absorption maximum) and exhibit additionally a pronounced shoulder around 720 nm (Figure 2B).

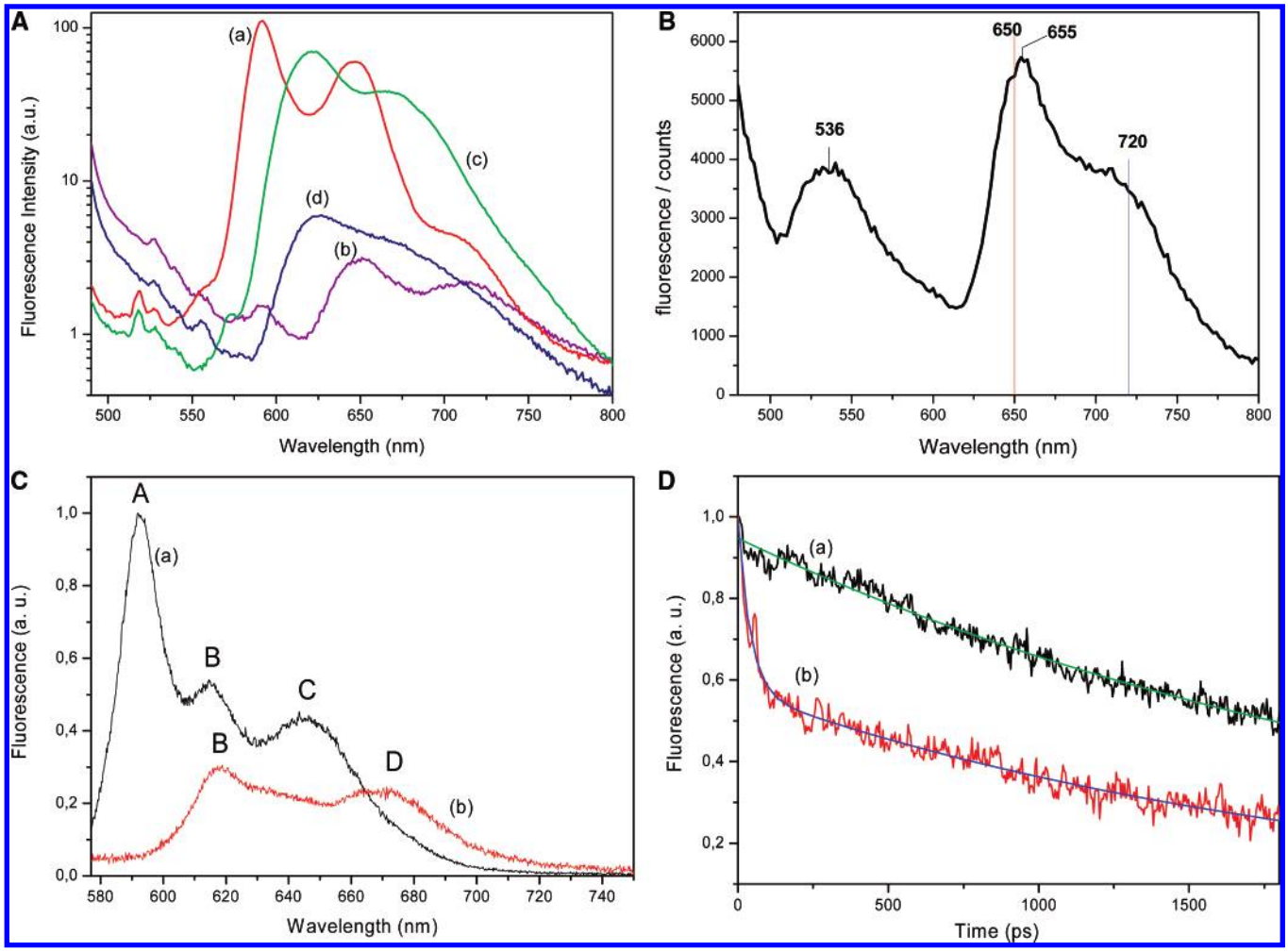

Figure 2. (A) Fluorescence of 0.15 mg of **1** dissolved in 10 μL of dry dichloromethane which was subsequently diluted in 1 mL of dry *n*-heptane. (a) Red trace, excitation at 420 nm; (b) porphyria trace, excitation at 480 nm. Then one drop of methanol was added to disrupt the self-assemblies: (c) green trace, excitation at 420 nm; (d) blue trace, excitation at 480 nm. Note that the blue trace differs considerably from the aggregate fluorescence curve (porphyria trace) and is due to excitation of **1**−methanol adducts. The smaller intensity of the blue trace in comparison to the green trace is due to the much reduced absorption of the **1**−methanol adducts at 480 nm. All spectra are not corrected for reabsorption or for the wavelength sensitivity of the detector. (B) Stationary fluorescence spectrum in the solid state of **1** on quartz deposited by spin-coating in a glovebox as a ~150 nm thick film. The spectrum is from the same sample as in Figure 1B with excitation at 405 nm. Note the shoulder at about 720 nm. Exclusion of oxygen during film formation is essential for obtaining a strong fluorescence signal. (C) Integrated fluorescence with excitation wavelengths at 430 nm (a, black trace) and 447 nm (b, red trace) from a self-assembled sample of **1** in *n*-heptane. (D) Decays of the fluorescence measured for peak A (from (C)) with excitation at 430 nm (a, black trace with the green curve representing the fit with $\tau_1 = 2.5$ ns) and for peak D (from (C)) with excitation at 447 nm (b, red trace with the blue curve representing the fit with $\tau_1 = 2.0$ ns and $\tau_2 = 40$ ps).

In Figure 2A we present the solution stationary fluorescence spectra of aggregated and monomeric **1**. Aggregates were formed by dilution into *n*-heptane, and one can selectively excite the monomers (at 420 nm) or the aggregates (at 480 nm). The fluorescence intensity of the monomers is at least 1 order of magnitude higher than that of the aggregates, which have a red-shifted maximum with a shoulder at ca. 720 nm. Note the very similar shape of the aggregate bands in solution (porphyria trace in Figure 2A) and in the solid state (Figure 2B). After addition of a very small amount of methanol, the aggregates are completely disassembled. Upon aggregation and especially in the solid state, chromophore fluorescence is strongly quenched and the lifetimes are usually drastically shortened. Typical monomer fluorescence decays measured for zinc porphyrins are on the order of about 2 ns.

Time-resolved-fluorescence measurements were performed on the aggregate suspensions of **1** in dry *n*-heptane where clearly one can selectively excite the monomers at 430 nm and the aggregates (excitation wavelength at 447 nm). Figure 2C shows the integrated fluorescence decays, while Figure 2D presents the fits for the decays recorded at the maxima for the monomers (peak A) and of the aggregates (peak D). While the decay for peak A can be well fitted by a single exponential with a lifetime of 2.5 ns, the decay of peak D is biexponential with a much faster component of 40 ps which can be ascribed to the aggregate induced fluorescence.

The fact that **1** fluoresces in the solid state is clear evidence of a very regular arrangement of the chromophores, just as in the chlorosomes for which extensive stationary fluorescence and time-resolved-fluorescence studies have been performed.[5,6] An estimation of the fluorescence quantum yield, taking also into account the relatively broad size distribution of the aggregates, is about 1 order of magnitude smaller than the zinc−monomer fluorescence, i.e., at ca. 0.5%. This sets limitations to using radiative processes for electron injection directly from the singlet excited state of the self-assemblies into the energetically matched conduction band of semiconductors (vide infra). The driving force can be tuned by adjusting the energy levels of the self-assembled chromophores to be higher than the conduction band of the semiconductors.

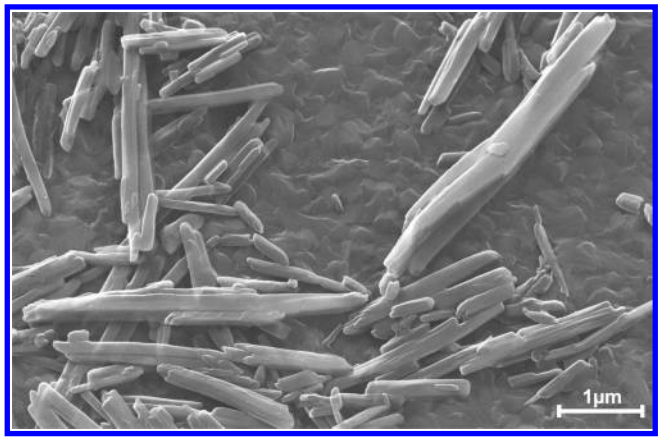

Figure 3. Scanning electron micrograph of a film cast from **1** on TiO_2, after annealing at 200 °C for 15 min. Accelerating voltage was 20 kV.

Figure 3 shows the scanning electron micrograph of the annealed film of **1** on TiO_2. This typical micrograph reveals the presence of large domains, with dimensions up to several micrometers, that consist of self-assembled stacks of **1**. The relative arrangement of stacks and monomers of **1** could not be deduced from such micrographs and is yet uncertain. Most probably, at the surface of the self-assemblies, monomers are present which are in direct contact with the semiconductor.

So far we could not grow crystals of **1** suitable for X-ray diffraction, but for the isomeric 15-acetyl-5-(1-hydroxyethyl)-10,20-bis(3,5-di-*tert*-butylphenyl)porphinato zinc (**2**) we could solve the structure within two different crystal modifications using synchrotron radiation.[7d,e] In both crystal modifications stacks of porphyrins are formed by the strong HO−Zn ligation combined with a weak electrostatic interaction on the other side of the tetrapyrrolic macrocycle between the acetyl group (>C═O) and the zinc atom. This 5 1/2 coordination of the zinc atoms ensures an orientation of the stacks as either down- or up-running. Only weak and multiple hydrophobic or dispersive forces are operating between the stacks, which pack differently in the two crystal modifications.[7d,e] Using small-angle X-ray scattering on powder samples and films, we could put into evidence strong reflexes between the self-assemblies of both isomeric **1** and **2** corresponding to 2.0 nm distances between zinc atoms which must be positioned in adjacent stacks. Using the coordinates determined for **2**, we could build a model for **1** applying the HyperChem molecular modeling package,[19] and after extensive geometry optimization, using alternatively a molecular mechanics force field (MM+) and a semiempirical force field (PM3), stacks were formed, three of which are shown in Figure 4. Note that either down- or up-running stacks (red arrows in Figure 4) can be packed side by side within the 2.0 nm spacing determined from the SAXS spectra. For self-assembled ^{13}C-labeled BChl *c*, which has three asymmetric carbon atoms and an additional stereogenic center at the magnesium atom,[20] such a diastereotopic stack orientation might explain the doubling of cross-peaks in the two-dimensional solid state ^{13}C NMR spectra recorded using radio frequency driven recoupling pulses at high spinning speeds under magic-angle conditions.[5h,j] Energy transfer within a stack is expected to be very fast, on a 100 fs time scale, while energy hopping between stacks should be on the picosecond time scale. Both processes are below the temporal resolution of our present measurements (ca. 8 ps).

Figure 5 shows the photoconductance transients of a bare spin-coated film of **1** on quartz, a bare TiO_2 film, and a bilayer of **1** on TiO_2 as spin-coated and after annealing. All measurements were obtained upon pulsed illumination at 430 nm. Since the electron mobility in TiO_2 largely exceeds the hole mobility in porphyrins,[21,23] an observed change in photoconductance predominantly results from an excess of mobile electrons present in the TiO_2 film. The initial rise of the photoconductance transients is due to the 18 ns instrumental response time.

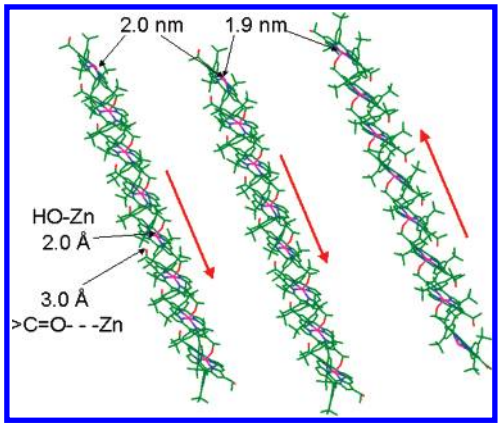

Figure 4. Three parallel running stacks shown as octamers of **1** at ca. 2.0 nm Zn−Zn distances. The acetyl group is tilted out of conjugation from the macrocyclic plane and points toward the Zn atom of a neighboring porphyrin. The up- or down-running stacks (red arrows) can pack by hydrophobic and dispersive forces, without hydrogen bonding, as proven for the crystal structures of **2** which served for building this computer model[19] of self-assembled **1**. Carbon atoms are green, oxygen red, nitrogen blue, and zinc purple. For an enlargement of a dimer, see the Supporting Information, Figure S5.

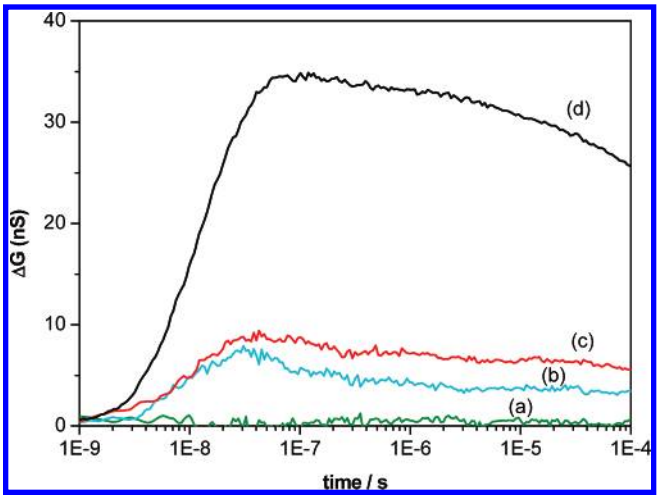

Figure 5. Photoconductance measurements upon laser excitation at 430 nm. (a) **1** self-assembled on a quartz substrate. (b) Bare TiO_2. (c) **1** self-assembled on TiO_2. (d) **1** self-assembled on TiO_2 after annealing.

Excitation of a film of **1** on quartz does not result in a detectable change in photoconductance. Pulsed illumination of bare TiO_2 results in a short-lived signal, which could be attributed to sub-band-gap excitation of electronic states present within the optical band gap.[22] In contrast, illumination of the annealed **1**/TiO_2 bilayer, in particular, results in a larger and longer lived change in photoconductance, which demonstrates photosensitization of TiO_2 by the film consisting of self-assembled **1**. Note that this photosensitization effect is considerably weaker for the nonannealed bilayer.

As discussed above, the OD spectrum of the **1**/TiO_2 bilayer reveals the presence of both self-assembled **1** stacks and nonassembled, monomeric **1**. In order to elucidate to which extent these two morphologically different features contribute to the formation of charge-separated states, the light-induced charge separation efficiency has been determined as a function

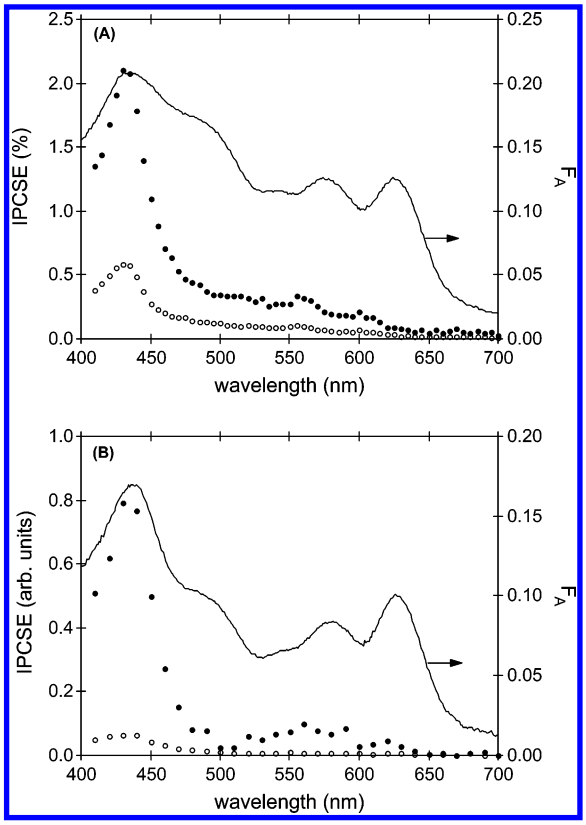

Figure 6. (A) Experimental IPCSE values of **1** on TiO_2 as spin-coated (open dots) and after annealing (solid dots) and the fraction of absorbed light F_A (solid, right ordinate axis) of the annealed bilayer. (B) Arbitrary IPCSE values for **1** on SnO_2, symbols are as in (A).

of excitation wavelength. Figure 6A shows the incident photon to charge separation efficiency (IPCSE) spectrum of **1** on TiO_2 as spin-coated and after annealing. Note that the shape of the IPCSE spectrum, in particular of the nonannealed bilayer, might be affected by a contribution originating from sub-band-gap excitation of TiO_2. Annealing causes the maximum IPCSE to increase from 0.6% to 2.2%; however, it hardly affects the shape of the IPCSE spectrum.

The enhanced light-induced charge separation efficiency realized upon annealing is caused by either an enlargement of the exciton diffusion length or an enhancement of the interfacial electron injection yield relative to all modes of interfacial exciton decay (ϕ_{inj}).[16] The only minor changes in the absorption spectrum indicate that annealing hardly affects the molecular organization. The enhanced light-induced charge separation efficiency obtained on annealing is therefore most likely caused by more efficient electron injection rather than by a longer exciton diffusion length. From comparison of the IPCSE spectrum of the annealed **1**/TiO_2 bilayer with the attenuation spectrum, also included in Figure 6A, it follows that the feature near 434 nm in the IPCSE spectrum due to absorption by monomeric **1** is significantly more pronounced than the features at 495, 575, and 628 nm caused by the self-assembled stacks of **1**. We therefore conclude that photons absorbed by the monomers are most effective to produce charge-separated states as these are probably located at the interface between the stacks and the semiconductor. Formation of charge-separated states is less efficient within the interior of the self-assembled stacks. Most probably, the large assemblies have an interface that has a monomer-like absorption spectrum and from these species an electron is injected into the TiO_2 conduction band.

Another possible reason for the low contribution of stacks to charge injection involves the energy of the exciton state, which might be too low for efficient electron injection into the conduction band of TiO_2. Although the monomers are present only in a relatively small amount, as judged from the residual peak of the Soret band, they may be the only ones capable of photosenzitization.

In order to elucidate whether this is the case, similar experiments have been performed using SnO_2 as the electron-accepting semiconductor. SnO_2 has a 0.6 eV higher electron affinity compared to TiO_2.[21] Figure 6B shows the IPCSE spectrum of **1** self-assembled on smooth SnO_2 as spin-coated and after annealing. Also included is the attenuation spectrum of the bilayer, which again shows the presence of both monomers and self-assembled stacks of **1**. As is also observed for TiO_2-based bilayers, the IPCSE of the **1**/SnO_2 bilayer increases significantly upon annealing. The shape of the IPCSE spectrum, both before and after annealing, is similar to those of the **1**/TiO_2 bilayer. This indicates that the inefficient conversion of excited states on self-assembled stacks of **1** into charge-separated states is most likely not due to the energy level of the exciton state. We are currently investigating by cyclic voltammetry the energy levels of **1**; however, this is a nontrivial experiment as it has to be performed practically in the absence of an electrolyte in order to prevent complete disassembly of the aggregates.

The former plausible explanation for a low contribution of self-assembled stacks of **1** to the formation of charge-separated states involves the exciton transfer between stacks and monomers present at the surface, which must be in partial contact with the semiconductor surface. Self-assembled stacks having red-shifted absorption maxima exhibit a smaller band gap compared to the surface monomers. Consequently, only exciton transfer from a monomer to a stack is energetically favorable, in contrast to the reverse energy transfer process. The observed IPCSE values on the order of 1−2% are typical for exciton diffusion over distances on the order of 1 nm,[16,23] corresponding to a few monolayers of molecules. The major contribution from nonassembled monomeric **1** to the formation of charge-separated states may originate from their presence at the surface of the electron-accepting semiconductor. Efficient conversion of excitons present on the self-assembled stacks of **1** into charge-separated states requires an ordered structure of stacks that are coated with an energetic trap that has to be in direct contact with the electron-accepting semiconductor. Methods to realize this are currently under investigation.

In conclusion, we have studied photosensitization of smooth TiO_2 and SnO_2 by an artificial self-assembling zinc porphyrin that mimics the natural chlorosomal bacteriochlorophylls. Self-assembly of these zinc porphyrin molecules results in the formation of large domains with dimensions up to several micrometers. In addition to self-assembled stacks, the porphyrin layer also contains nonassembled zinc porphyrin monomers, probably at the stack−semiconductor interface. Photosensitization of semiconductors in hybrid bilayers using our bioinspired chromophores with built-in self-assembly features must be improved in future constructs. At present, predominantly those photons absorbed by the monomers lead to the formation of charge-separated states. The low contribution of self-assembled stacks to the formation of charge-separated states most likely originates from the nonoptimized interaction with the semiconductor, combined with the presence of monomers at the semiconductor surface and the energetically unfavorable exciton transfer from a stack to a monomer. Realizing an ordered structure of stacks, coated by other chromophores that are able to act as traps for energy transfer and at the same time have an

appropriate contact with the electron-accepting semiconductor, possibly will enhance the formation of charge-separated states.

Acknowledgment. W. M. Gnehr, Fraunhofer Institut Elektronenstrahl- und Plasmatechnik, Dresden, Germany, is acknowledged for the generous gift of the SnO_2 substrates. Research in Delft was supported financially by the Delft Research Centre for Sustainable Energy. Research in Karlsruhe was partially supported by the DFG Center for Functional Nanostructures (CFN) at the University of Karlsruhe through former projects C3.2 and C3.6 and current project C3.5.

Supporting Information Available: Experimental details, thermal and electron beam stability tests, details of the supramolecular interactions in a dimer of **1**. This material is available free of charge via the Internet at http://pubs.acs.org.

References and Notes

(1) (a) Blankensip, R. E. *Molecular Mechanisms of Photosynthesis*; Blackwell Science: Oxford, 2002. (b) LH2: McDermott, G.; Prince, S. M.; Freer, A. A.; Hawthornthwaite-Lawless, A. M.; Papiz, M. Z.; Cogdell, R. J.; Isaacs, N. W. *Nature* **1995**, *374*, 517−521. (c) LH2 at 2.0 Å: Papiz, M. Z.; Prince, S. M.; Howard, T.; Cogdell, R. J.; Isaacs, N. W. *J. Mol. Biol.* **2003**, *326*, 1523−1538. (d) LH2−RC: Roszak, A. W.; Howard, T. D.; Southall, J.; Gardiner, A. T.; Law, C. J.; Isaacs, N. W.; Cogdell, R. J. *Science* **2003**, *302*, 1969−1972. (e) PS I: Jordan, P.; Fromme, P.; Witt, H.-T.; Klukas, O.; Saenger, W.; Krauss, N. *Nature* **2001**, *411*, 909−917. (f) PS I−LHC I: Ben-Shem, A.; Frolow, F.; Nelson, N. *Nature* **2003**, *426*, 630−635. (g) PS II at 3.0 Å: Loll, B.; Kern, J.; Saenger, W.; Zouni, A.; Biesiadka, J. *Nature* **2005**, *438*, 1040−1044. (h) LHC II at 2.7 Å: Liu, Z.; Yan, H.; Wang, K.; Kuang, J.; Gui, L.; An, X.; Chang, W. *Nature* **2004**, *428*, 287−292. (i) FMO: Fenna, R. E.; Mathews, B. W. *Nature* **1975**, *258*, 573−577. (j) FMO at 2.2 Å: Camara-Artigas, A.; Blankenship, R. E.; Allen, J. P. *Photosynth. Res.* **2003**, *75*, 49−55. (k) FMO−BChl *a* assignments: Brixner, T.; Stenger, J.; Vaswani, H. M.; Cho, M.; Blankenship, R. E.; Fleming, G. R. *Nature* **2005**, *434*, 625−628.

(2) van Grondelle, R.; Dekker, J. P.; Gillbro, T.; Sundstrom, V. *Biochim. Biophys. Acta* **1994**, *1187*, 1−65.

(3) (a) Staehelin, L. A.; Golecki, J. R.; Fuller, R. C.; Drews, G. *Arch. Mikrobiol.* **1978**, *119*, 269−277. (b) Staehelin, L. A.; Golecki, J. R.; Drews, G. *Biochim. Biophys. Acta* **1980**, *589*, 30−45. (c) Saga, Y.; Tamiaki, H. *J. Biosci. Bioeng.* **2006**, *102*, 118−123.

(4) (a) Bystrova, M. I.; Mal'gosheva, I. N.; Krasnovskii, A. A. *Mol. Biol.* **1979**, *13*, 440−451. (b) Smith, K. M.; Kehres, L. A.; Fajer, J. *J. Am. Chem. Soc.* **1983**, *105*, 1387−1389. (c) Brune, D. C.; Nozawa, T.; Blankenship, R. E. *Biochemistry* **1987**, *26*, 8644−8652.

(5) (a) Holzwarth, A. R.; Griebenow, K.; Schaffner, K. *Z. Naturforsch.* **1990**, *45c*, 203−206. (b) Griebenow, K.; Holzwarth, A. R.; van Mourik, F.; van Grondelle, R. *Biochim. Biophys. Acta* **1991**, *1058*, 194−202. (c) Alden, R. G.; Lin, S. H.; Blankenship, R. E. *J. Lumin.* **1992**, *51*, 51−66. (d) Nozawa, T.; Ohtomo, K.; Suzuki, M.; Nakagawa, H.; Shikama, Y.; Konami, H.; Wang, Z.-Y. *Photosynth. Res.* **1994**, *41*, 211−223. (e) Balaban, T. S.; Holzwarth, A. R.; Schaffner, K.; Boender, G. J.; Degroot, H. J. M. *Biochemistry* **1995**, *34*, 15259−15266. (f) Chiefari, J.; Griebenow, K.; Fages, F.; Griebenow, N.; Balaban, T. S.; Holzwarth, A. R.; Schaffner, K. *J. Phys. Chem. B* **1995**, *99*, 1357−1365. (g) Wang, Z.-Y.; Umetsu, M.; Yoza, K.; Kobayashi, M.; Imai, M.; Matsushita, Y.; Niimura, N.; Nozawa, T. *Biochim. Biophys. Acta* **1997**, *1320*, 73−82. (h) Balaban, T. S.; Tamiaki, H.; Holzwarth, A. R.; Schaffner, K. *J. Phys. Chem. B* **1997**, *101*, 3424−3431. (h) van Rossum, B. J.; Boender, G. J.; Mulder, F. M.; Raap, J.; Balaban, T. S.; Holzwarth, A. R.; Schaffner, K.; Prytulla, S.; Oschkinat, H.; de Groot, H. J. M. *Spectrochim. Acta, Part A: Mol. Biomol. Spectrosc.* **1998**, *54*, 1167−1176. (i) Balaban, T. S.; Leitich, J.; Holzwarth, A. R.; Schaffner, K. *J. Phys. Chem. B* **2000**, *104*, 1362−1372. (j) van Rossum, B. J.; Steensgaard, D. B.; Mulder, F. M.; Boender, G. J.; Schaffner, K.; Holzwarth, A. R.; de Groot, H. J. M. *Biochemistry* **2001**, *40*, 1587−1595. (k) de Boer, I.; Matysik, J.; Amakawa, M.; Yagai, S.; Tamiaki, H.; Holzwarth, A. R.; de Groot, H. J. M. *J. Am. Chem. Soc.* **2003**, *125*, 13374−13375. (l) Pšenčik, J.; Ikonen, T. P.; Laurinmaki, P.; Merckel, M. C.; Butcher, S. J.; Serimaa, R. E.; Tuma, R. *Biophys. J.* **2004**, *87*, 1165−1172. (m) Balaban, T. S. Light-harvesting Nanostructures. In *Encyclopedia of Nanoscience and Nanotechnology*; Nalwa, H. S., Ed.; American Scientific Publishers: Los Angeles, 2004; Vol. 4, pp 505−559. (n) Balaban, T. S.; Tamiaki, H.; Holzwarth, A. R. Chlorins Programmed for Self-assembly. In *Supramolecular Dye Chemistry*; Würthner, F., Ed.; Topics in Current Chemistry 258; Springer-Verlag: Berlin, 2005; pp 1−38.

(6) (a) Blankenship, R. E.; Brune, D. C.; Wittmershaus, B. P. Chlorosome antennas in green photosynthetic bacteria. In *Light-energy transduction in photosynthesis: higher plant and bacterial models*; Stevens, S. E., Bryant, D. A., Eds.; American Society of Plant Physiologists: Rockville, MD, 1988; pp 32−46. (b) Frigaard, N. U.; Chew, A. G. M.; Li, H.; Maresca, J. A.; Bryant, D. A. *Photosynth. Res.* **2003**, *78*, 93−117. (c) Frigaard, N. U.; Bryant, D. A. Chlorosomes: Antenna Organelles in Photosynthetic Green Bacteria. In *Complex Intracellular Structures in Prokaryotes*; Microbiology Monographs 2; Shively, J. M., Ed.; Springer-Verlag: Berlin, 2006; pp 79−114.

(7) (a) Balaban, T. S.; Bhise, A. D.; Fischer, M.; Linke-Schaetzel, M.; Roussel, C.; Vanthuyne, N. *Angew. Chem., Int. Ed.* **2003**, *42*, 2140−2144. (b) Balaban, T. S.; Linke-Schaetzel, M.; Bhise, A. D.; Vanthuyne, N.; Roussel, C. *Eur. J. Org. Chem.* **2004**, 3919−3930. (c) Linke-Schaetzel, M.; Bhise, A. D.; Gliemann, H.; Koch, Th.; Schimmel, Th.; Balaban, T. S. *Thin Solid Films* **2004**, *451*−*452*, 16−21. (d) Balaban, T. S.; Linke-Schaetzel, M.; Bhise, A. D.; Vanthuyne, N.; Roussel, C.; Anson, C. E.; Buth, G.; Eichhöfer, A.; Foster, K.; Garab, G.; Gliemann, H.; Goddard, R.; Javorfi, T.; Powell, A. K.; Rösner, H.; Schimmel, Th. *Chem.—Eur. J.* **2005**, *11*, 2267−2275. (e) Balaban, T. S. *Acc. Chem. Res.* **2005**, *38*, 612−623.

(8) *The Porphyrin Handbook*; Kadish, K., Smith, K. M., Guillard, R., Eds.; Academic Press: San Diego, 2000; Vol. 1.

(9) (a) Overmann, J.; Cypionka, H.; Pfennig, N. *Limnol. Oceanogr.* **1992**, *37*, 150−155. (b) Beatty, J. T.; Overmann, J.; Lince, M. T.; Manske, A. K.; Lang, A. S.; Blankenship, R. E.; Van Dover, C. L.; Martinson, T. A.; Plumley, F. G. *Proc. Natl. Acad. Sci. U.S.A.* **2005**, *102*, 9306−9310.

(10) (a) Grätzel, M. *Nature* **2001**, *414*, 338−344. (b) Gregg, B. A. *J. Phys. Chem. B* **2003**, *107*, 4688−4698.

(11) (a) Haque, S. A.; Tachibana, Y.; Willis, R. L.; Moser, J. E.; Grätzel, M.; Klug, D. R.; Durrant, J. R. *J. Phys. Chem. B* **2000**, *104*, 538−547. (b) Haque, S. A.; Handa, S.; Peter, K.; Palomares, E.; Thelakkat, M.; Durrant, J. R. *Angew. Chem., Int. Ed.* **2005**, *44*, 5740−5744.

(12) (a) O'Regan, B.; Grätzel, M. *Nature* **1991**, *353*, 737−740. (b) Grätzel, M. *Prog. Photovoltaics Res.* **2006**, *14*, 429−442. (c) For a recent summary of performances in photovoltaics, see: Green, M. A.; Emery, K.; King, D. L.; Hishikawa, Y.; Warta, W. *Photovoltaics Res.* **2006**, *14*, 455−461.

(13) (a) Schmidt-Mende, L.; Zakeeruddin, S. M.; Grätzel, M. *Appl. Phys. Lett.* **2005**, *86*, 013504. (b) Schmidt-Mende, L.; Bach, U.; Humphry-Baker, R.; Horiuchi, T.; Miura, S.; Ito, S.; Uchida, S.; Grätzel, M. *Adv. Mater.* **2005**, *17*, 813−815. (c) Hoppe, H.; Sariciftci, N. S. *J. Mater. Chem.* **2006**, *16*, 45−61. (d) Schraber, M. C.; Mühlbacher, D.; Koppe, M.; Denk, P.; Waldauf, C.; Heeger, A. J.; Brabec, C. J. *Adv. Mater.* **2006**, *16*, 789−794.

(14) Ito, S.; Ngoc-Le, C. H.; Rothenberger, G.; Liska, P.; Compte, P.; Zakeeruddin, S. M.; Péchy, P.; Nazeeruddin, M. K.; Grätzel, M. *Chem. Commun.* **2006**, 4004−4006.

(15) Nelson, J.; Chandler, R. E. *Coord. Chem. Rev.* **2004**, *248*, 1181−1194.

(16) (a) De Haas, M. P.; Warman, J. M. *Chem. Phys.* **1982**, *73*, 35−53. (b) Kroeze, J. E.; Savenije, T. J.; Vermeulen, M. J. W.; Warman, J. M. *J. Phys. Chem. B* **2003**, *107*, 7696−7705. (c) Kroeze, J. E.; Savenije, T. J.; Warman, J. M. *J. Am. Chem. Soc.* **2004**, *126*, 7608−7618. (d) Huijser, A.; Savenije, T. J.; Kroeze, J. E.; Siebbeles, L. D. A. *J. Phys. Chem. B* **2005**, *109*, 20166−20173.

(17) Gouterman, M. In *The Porphyrins*; Dolphin, D., Ed.; Academic Press: New York, 1978; Vol. III, Part A, Physical Chemistry.

(18) For recent pertinent references concerning J-aggregates (also called Jelly or Schiebe aggregates), see: (a) Dähne, L. *J. Am. Chem. Soc.* **1995**, *117*, 12855−12860. (b) Wang, M.; Silva, G. L.; Armitage, B. A. *J. Am. Chem. Soc.* **2000**, *122*, 9977−9986. (c) Okada, S.; Segawa, H. *J. Am. Chem. Soc.* **2003**, *125*, 2792−2796.

(19) *HyperChem*, Professional Edition, Release 7.5; Hypercube Inc.: Gainesville, FL, 2003.

(20) (a) Balaban, T. S.; Holzwarth, A. R.; Schaffner, K. *J. Mol. Struct.* **1995**, *349*, 183−186. (b) Balaban, T. S.; Fromme, P.; Holzwarth, A. R.; Krauss, N.; Prokhorenko, V. I. *Biochim. Biophys. Acta (Bioenergetics)* **2002**, *1556*, 197−207. (c) Balaban, T. S. *FEBS Lett.* **2003**, *545*, 97−102; Erratum *FEBS Lett.* **2003**, *547*, 235. (d) Balaban, T. S. *Photosynth. Res.* **2005**, *86*, 251−262.

(21) Bak, T.; Nowotny, J.; Rekas, M.; Sorrell, C. C. *J. Phys. Chem. Solids* **2003**, *64*, 1069−1087.

(22) Checcoli, P.; Conte, G.; Salvatori, S.; Paolesse, R.; Bolognesi, A.; Berliocchi, A.; Brunetti, F.; D'Amico, A.; Di Carlo, A.; Lugli, P. *Synth. Met.* **2003**, *138*, 261−266.

(23) Kroeze, J. E.; Savenije, T. J.; Warman, J. M. *J. Photochem. Photobiol., A: Chem.* **2002**, *148*, 49−55.